Research article

Development of bioactive resin modified glass ionomer cement for dental biomedical applications

Ika Dewi Ana [a],[*], Rahmi Anggraeni [b]

[a] Department of Dental Biomedical Sciences, Faculty of Dentistry, Universitas Gadjah Mada, Yogyakarta 55281, Indonesia
[b] PT Swayasa Prakarsa, UGM Science Techno Campus, Division of Drugs, Medical Devices, and Functional Food, Yogyakarta 55571, Indonesia

ABSTRACT

It would certainly be an advantage of resin-modified glass ionomer cement (RMGIC) if it can possess bioactivity. However, research related to that is still very limited. Hybridization of RMGIC was predicted to increase mechanical properties and resistance to disintegration, and low content of polyacrylic acid induces cement bioactivity. This study investigated the effect of BAG obtained from the $CaSiO_3–Ca_3(PO_4)_2$ system on RMGIC bioactivity. BAG samples containing 10%, 15%, and 20% P_2O_5 (denoted as "CSP10," "CSP15," and "CSP20," respectively) were used to modify RMGIC powder, and apatite wollastonite was used for comparison. Surface bioactivity was assessed using XRD pattern, infrared spectroscopy, and SEM microstructure after specimen immersion in simulated body fluid (SBF). Contents of Ca, P, F, Sr, and Al were measured in the remaining SBF. Cell attachment, proliferation, and differentiation on the RMGIC containing BAG were evaluated and compared with those on the RMGIC without BAG. Sr and Al analyses revealed that the addition of BAG may not influence the matrix stability of the cement. Moreover, the addition of BAG was a positive factor indicating excellent ion exchange in SBF and spontaneous growth of apatite by consuming the Ca and P ions in the surrounding fluid. Osteoblast differentiation was higher on the four types of bioactive cements than on the RMGIC without BAG. The results of these studies provide novel insights into the development of a new generation of osteoconductive biomedical materials.

1. Introduction

Glass ionomer cement (GIC) has various dental applications. Different from other restorative materials, with no additional bonding agent GIC can be placed directly into tooth cavities and has fluoride releasing property [1, 2, 3, 4]. However, at the initial stage of setting GIC is known to be sensitive to water. Exposure of GIC paste to saliva at the initial stage of setting decreases its mechanical strength significantly. Conventional GIC was then modified by water-soluble resin [5] and called "resin-modified glass ionomer cement (RMGIC)". The liquid phase of RMGIC is composed of polycarboxylic acid, 2-hydroxyethylmethacrylate (HEMA), and water. Meanwhile, the composition of the powder phase of RMGIC is the same as that of conventional GIC. In the conventional GIC (fluoroaminosilicate glass), the powder composition allows the glass to react with the weak acid (poly-carboxylic acid) inside the glass system [6].

Nowadays, GIC is being developed for bone replacements and wide biomedical applications [7, 8, 9, 10, 11, 12]. Hence, bioactivity in term of the ability to form apatite [13] is an important factor for the successful application of GIC. However, even if the powder phase of RMGIC contains calcium and phosphate, RMGIC still does not show any bioactivity. Bioactivity induction in RMGIC would be advantageous in regenerative dentistry, but limited research has been performed so far.

Matsuya et al. [10] reported a new GIC based on the composition of bioactive $CaO–P_2O_5–SiO_2(-MgO)$ glass and investigated its setting related processes. They found that carboxylate salt forms as Ca^{2+} is released from bioactive glass (BAG) and that polymerization degree increases in the silicate network. The essential setting mechanism of the bioactive $CaO–P_2O_5–SiO_2(-MgO)$ glass was found through an acid–base reaction between the basic glass and the polymeric acid is the same as that in the GIC. However, the compressive strength of the set bioactive $CaO–P_2O_5–SiO_2(-MgO)$ glass is much lower than that of the GIC. The set cement also disintegrates during SBF immersion. They also evaluated the bioactivity of the cement in simulated body fluid (SBF) and found no apatite was formed on the surface of the new set bioactive $CaO–P_2O_5–SiO_2(-MgO)$ glass at least within 4 weeks. Kamitakahara et al. evaluated whether it was possible to obtain bioactive GIC in the presence

or absence of polyacrylic acid [14]. They found that apatite formation on SBF-immersed BAG is suppressed in the presence of 0.1 ppm polyacrylic acid and that GIC bioactivity is inhibited. This result indicates that polyacrylic acid or acid in general suppresses the apatite formation of BAG.

Hybridization of RMGIC and BAG overcomes the limitations of the conventional GIC because RMGIC has less polyacrylic acid concentration than the conventional GIC. The lesser concentration of polyacrylic acid is due to the rapid set of RMGIC by HEMA or methacrylate group polymerization in the polyacid chain. Modification of GIC by resin component inclusion in the RMGIC cement can increase mechanical strength and resistance to disintegration. Ana *et al.* [15] showed that inclusion of four types of BAG into a commercially available RMGIC is clinically acceptable. Excellent setting ability is provided by the inclusion of BAG into RMGIC [15]. They concluded that bioactive RMGIC can be developed for clinical applications. However, the bioactivity of RMGIC has yet to be evaluated.

In the present study, BAG was combined in 50% weight ratios with the powder phase of RMGIC and examined for the possibility of obtaining bioactive RMGIC. Apatite forms of the cements immersed in SBF were investigated by the pattern of X-ray diffraction (XRD), spectroscopy of FT-IR, chemical analysis, and microstructural analysis. Cell studies were also performed to predict its biocompatibility and bioactivity.

2. Materials and methods

2.1. Preparation of bioactive powders

Four types of bioactive glass powders (Table 1) were developed as described in a previous study [15]. BAG powders obtained from the glass $CaSiO_3$–$Ca_3(PO_4)_2$ system were used to achieve 10, 15, and 20 weight% P_2O_5 contents, which were then denoted as "CSP10," "CSP15," and "CSP20." For comparison, apatite wollastonite glass ceramics without CaF_2 was prepared as reported by Kokubo [12] and denoted as "AWG".

2.2. Preparation of RMGIC containing BAG

RMGIC containing BAG was prepared by adding BAG into the powder phase of RMGIC (Fuji II LC, GC Corp., Tokyo, Japan), denoted as "FLC" in the following text. The detailed composition of Fuji II LC powder phase is not publicly open, but reports show that the powder is free from polycarboxylic acid. The FLC and BAG powders were mixed to achieve 50 weight% BAG contents. The prepared cement powders are denoted on the basis of the BAG added and its percentage in parentheses: CSP10(50), CSP15(50), CSP20(50), and AWG(50). Without any modification, Fuji II LC liquid was used and applied as the liquid phase of BAG-containing cement for simplicity. The powder of the studied FLC and bioactive RMGICs were mixed with Fuji II LC liquid and poured into Teflon molds in 6 mm diameter by 0.7 mm thickness for bioactivity test in SBF, 10 mm diameter by 0.1 mm thickness for cell attachment test, and 6 mm diameter by 0.7 mm thickness for cell proliferation and differentiation test. After 2 min from the start of the mixing, light irradiation was performed for 2 × 20 s using light curing unit (Lightel DP 075, Morita Corp., Tokyo, Japan). Specimens were then incubated at 37 °C and 100% humidity for 24 h to allow them to set completely. The preparation of RMGIC containing BAG was performed as previously described [15].

2.3. Immersion in SBF

Disk specimens were soaked for various periods in 20 mL of SBF at 37degree Celsius to test bioactivity in vitro. The SBF was prepared to reach human blood plasma ion concentrations at 7.4 pH. The SBF solutions used in this study contained ion concentrations as those provided by Kokubo [16] as described in Table 2. After 0, 1, 2, 4, and 8 weeks, the specimens were washed with distilled water, dried, and then prepared for analysis.

2.4. Surface analysis after immersion

The specimens were studied using XRD to confirm whether apatite was present after the SBF immersion for various periods at a typical scan step of 2θ equivalent to 0.02° and scan speed of 2°/min. A Cu Kα tube operating at 40 kV and 100 mA was used for the generation of X-ray (RINT 2500V, Rigaku Co., Tokyo, Japan). The specimen surface was gold sputtered using JEC 550 Twin Coater (JEOL, Tokyo, Japan) and then examined under a JSM 5400 LV (JEOL, Tokyo, Japan) scanning electron microscope to confirm whether apatite was formed on the surface of RMGIC containing BAG. FT-IR spectroscopy was applied to the ground surface to assess the type of apatite formation on the specimen surface. The transmission spectra of FT-IR were obtained using an IR spectrometer (Spectrum 2000, The Perkin- Elmer Co., CT, USA) by the KBr disk method.

2.5. Chemical analysis of immersion solution

The SBF used for immersion was analyzed for pH, fluoride, aluminum, strontium, calcium, and phosphate before and after the specimen's immersion. Level of pH was determined using a glass pH meter (TPX-90, Toko Chemical Lab. Co. Ltd., Tokyo, Japan). An ion specific combination electrode (model 720A plus, Orion research, Cambridge, MA) was used to analyzed fluoride concentration. At a specific time, a 2 mL aliquot of each sample was placed in a plastic cup for fluoride concentration measurement. To adjust ionic strength and pH, 2 mL of 10 times diluted TISAB III solution (Orion research, Cambridge, MA) was mixed with the samples. The fluoride electrode calibration was conducted before each measurement by using the same sample solution mixed with 2 mL of solutions containing 0.1, 0.2, 0.5, 1, and 5 ppm fluoride. Remeasurement was conducted to always give less than 10% concentration difference.

Atomic absorption spectroscopy (Analyst 300, The PerkinElmer Co., Tokyo, Japan) was applied to determine calcium (Ca 422.7 nm), aluminum (Al 309.3 nm), and strontium (Sr 460.7 nm) concentrations with C_2H_2/N_2O, C_2H_2/N_2O, and C_2H_2/air flame respectively. A 1 mol/L hydrochloric acid and 1 mL of 1% KCl was mixed with 0.5 mL aliquot of SBF solution to suppress ionization interference for the Ca analysis after immersion. The SBF solution without Ca was also prepared as standard solution with 2.0–5.0 ppm for Ca analysis. Meanwhile, 5 mL of each sample was mixed with 1 mL of 1 mol/L hydrochloric acid and 1 mL of 1% KCl to analyze Al and Sr by suppressing ionization interference. Standard solutions for Al and Sr were 0.1–5.0 ppm, and those for Ca were 2.0–5 ppm. Each measurement was conducted in triplicate, before averaging the concentration values. Standard deviation was always set up less than 5%. The Ca concentration from each specimen was expressed

Table 1. Composition of BAG prepared in the study (in mol%) as referred to the previous study [14].

Glass	CaO	SiO$_2$	P$_2$O$_5$	MgO	Remarks
CSP10	54.3	41.3	4.3	-	CaSiO$_3$–Ca$_3$(PO$_4$)$_2$ 10wt% as P$_2$O$_5$
CSP15	56.7	36.6	6.7	-	CaSiO$_3$–Ca$_3$(PO$_4$)$_2$ 15wt% as P$_2$O$_5$
CSP20	59.2	31.6	9.2	-	CaSiO$_3$–Ca$_3$(PO$_4$)$_2$ 20wt% as P$_2$O$_5$
AWG	50.1	35.6	7.2	7.1	CaSiO$_3$–Ca$_3$(PO$_4$)$_2$ 16.4wt% as P$_2$O$_5$

Table 2. Chemical composition of SBF [15].

Order	Reagent	Amount (g/L)
1.	NaCl	7.996
2.	NaHCO$_3$	0.350
3.	KCl	0.224
4.	K$_2$HPO$_4$.3H$_2$O	0.228
5.	MgCl$_2$.6H$_2$O	0.305
6.	1 mol/L HCl	40cm^3
7.	CaCl$_2$	0.278
8.	Na$_2$SO$_4$	0.071
9.	(CH$_2$OH)$_3$CNH$_2$	6.057
10.	1 mol/L HCl	Adjust pH by dropping

as ppm. The amount of each Al and Sr released was expressed as a cumulative amount per unit surface area of specimen disk (μg/cm^2).

The phosphate concentration of each SBF solution after immersion was analyzed using an ultraviolet/visible light spectrometer (UV/VIS spectrometer, U-best 50, JASCO, Tokyo, Japan), in which 1 mL of each sample was mixed with 1 mL of Na$_2$MoO$_4 \cdot$2H$_2$O 2.5 g/L and 1 mL of 0.5 N$_2$H$_6$SO$_4$. A standard solution of P was prepared from KH$_2$PO$_4$ with concentrations of 0.5–2.0 ppm. Five times measurement were conducted for each specimens, and the concentration values were expressed in mean $\pm$ SD. The P concentration from each specimen was expressed as ppm.

2.6. Cell attachment, proliferation, and differentiation

Osteoblast-like cells (MC3T3E1) were used in this study to confirm bioactivity. Cells were obtained from Gibco (USA). The culture medium was α-MEM (Eagle, Sigma Chemical Co., St. Louis, MO, USA) with 10% fetal bovine serum (Gibco, Invitrogen Co., Auckland, New Zealand) in an atmospheric conditioned containing 5% CO$_2$ at 37 $^\circ$C. Cells were seeded on each disk in a number of 1×10^4 cells per 10 mm disk, and plastic dishes (24-well cell culture cluster, Corning, New York, USA) containing no osteoblasts were used as the control.

The cells were seeded onto FLC and cements contaning BAG followed by 5 h incubation. After 5 h incubation, 0.1 mol/L phosphate buffer saline washing was conducted to eliminate non-adherent cells. The adherent osteoblasts on the specimens were harvested for cell attachment

Figure 1. X-ray diffraction pattern of resin-modified glass ionomer cement (FLC) after immersion in SBF at various times up to 8 weeks.

report and then counted using a Burker and Turk hemocytometer. The PBS containing collagenase and trypsin was prepared for adherent cell harvesting. Cell proliferation was measured at 1, 3, 5, 7, and 9 days using 3[4,5-dimethylthiazole-2-yl]2,5-diphenyltetrazolium bromide (MTT) assay. Absorbance was determined at 570 nm using a plate reader (MTP-32 Microplate Reader, Corona Elect., Ibaragi, Japan), following the method as previously described by Yuasa et al. [17].

The determination of alkaline phosphatase (ALP) activity of the osteoblasts on days 6, 9, and 12 was analyzed by enzyme-linked immunosorbent assay (ELISA) using p-nitrophenyl phosphate as the substrate with the p-nitrophenol absorbance at 405 nm in a plate reader (MTP- 32 Microplate Reader, Corona Elect., Ibaragi, Japan). Enzymatic activity was expressed as nmol of p-nitrophenol/minute per mg protein. Bradford assay (1976) using bovine- γ-globulin as a standard was applied to determine protein content [17, 18].

For type I procollagen peptide (PICP) and osteocalcin analysis, each specimen was decalcified with 0.6 mmol/L HCl for 30 min. The assay was conducted to the harvested solution upon storage at -20 $^\circ$C. The PICP amounts on days 3, 9, and 12 and osteocalcin on days 9, 15, and 21 were measured with an ELISA kit (Takara, Shiga, Japan).

2.7. Statistical analysis

One-way ANOVA and Fischer's PLSD method as post-hoc- test were performed for statistical analysis. Statistical significance was considered at $p < 0.05$.

3. Results

3.1. Surface analysis on the bioactivity of the set cement

Bioactivity could be evaluated by the apatite formation on the cement surface after immersion in SBF. Figures 1 and 2 show the XRD patterns of FLC (RMGIC without BAG) as a control and those of the cements containing 50 weight% of CSP10, CSP15, CSP20, and AWG after various immersion times in SBF, with hydroxyapatite (HAP) diffraction pattern as a reference. With the control FLC, no apatite peak was observed at any period of immersion (Figure 1). Diffraction patterns for the cements containing BAGs showed two broad diffraction peaks at around 25.5° and 32.0°, which were assigned to the apatite phase [19, 20] after 4 or 8 weeks of immersion on the surfaces of CSP10(50), CSP15(50), and CSP20(50) and after 8 weeks of immersion on the surface of AWG(50).

Bioactivity of the cements containing BAGs was also detected by microstructure of the specimens observed with SEM. Figure 3 shows a surface micrograph of the specimens FLC, CSP10 in 50 weight%, and AWG in 50 weight%. As confirmed from the XRD patterns shown in Figures 1 and 2, Figure 3 confirms that a spherical poorly crystalline apatite layer formed on the cement surface after immersion for four and/ or 8 weeks. With FLC, no crystalline materials were observed even after immersion for 8 weeks, as expected from the XRD result.

As shown in Figure 4, the FT-IR spectra of FLC did not change before and after immersion, except for an increase in peak intensity at 1563 cm^{-1}, which was assigned to the asymmetric vibration of carboxylate. Meanwhile, the FT-IR spectra of CSP10(50) showed new absorption bands around 873, 602, and 568 cm^{-1}, which were assigned to CO$_3$ and PO$_4$ in carbonated apatite, aside from the asymmetric stretching vibration of the carboxylates at 1563 cm^{-1}. The bands at 1460 and 1415 cm^{-1} assigned to CO$_3$ in B- type carbonated apatite overlapped with those from the symmetric vibration mode of the carboxyl group and ester in the original cement FLC. However, the intensity of the absorption bands increased, which clearly showed the formation of carbonated apatite after immersion. Together with CSP10(50) and FLC, CSP15(50), CSP20(50), and AWG(50) also revealed similar changes in their FT-IR spectra (Figure 5). Table 3 summarizes the confirmation on the apatite formation by XRD, FT-IR, and SEM.
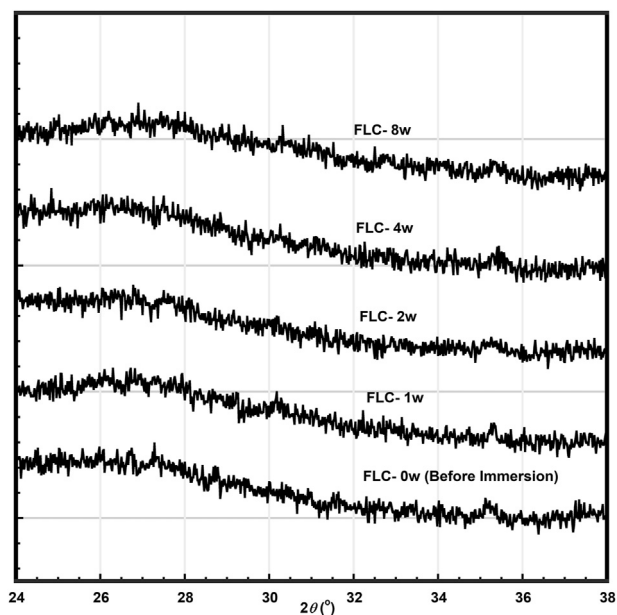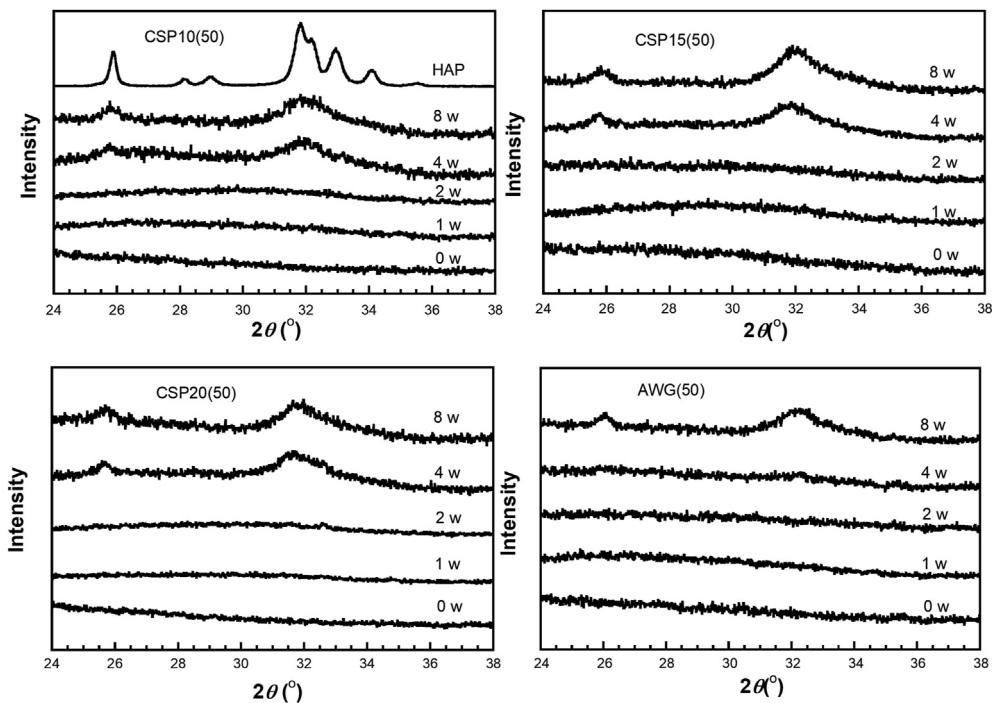
Figure 2. X-ray diffraction pattern of resin-modified glass ionomer cements containing bioactive glasses CSP10(50), CSP15(50), CSP20(50), and AWG after immersion in SBF at various times up to 8 weeks. HAP shows diffraction of synthetic hydroxyapatite.
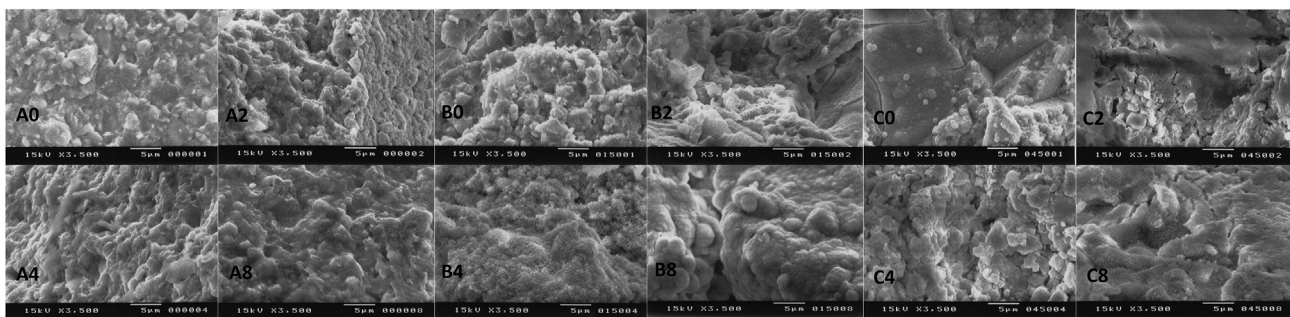

Figure 3. Scanning electron micrograph representatives of (A) resin-modified glass ionomer cement (FLC), (B) CSP10(50), and (C) AWG after 0, 2, 4, and 8 of weeks immersion in SBF.

3.2. Calcium and phosphate concentrations in SBF solution

Figures 6 and 7 show the Ca^{2+} and PO_4^{3-} ions concentration in SBF after certain periods of immersions. Calcium concentrations increased significantly by the addition of CSP10(50) up to the 4 weeks of immersion, slightly increased in CSP15(50), CSP20(50), and AWG(50), but it was stabilized in FLC. Meanwhile, phosphate concentrations tend to decrease significantly with the addition of BAGs but it was also stabilized in FLC. No significant changes in pH level were observed during this study. The pH level ranged from 7.4 to 8.1.

3.3. F, Sr, and Al releases from the cement

Figures 8, 9, and 10 show the log-log plots for fluoride, strontium, and aluminum released from the various cements containing 50% BAGs after immersion in SBF. The amount of F released into SBF decreased with glass addition. This finding is reasonable because the added BAG does not contain any fluoride ions. Thus, the released fluoride must have originated entirely from the powder component of RMGIC. The amount of fluoride releases also differed among the BAG types. Although the amount of fluoride released from RMGIC containing BAG was lower than

that released from FLC, the bioactive RMGIC presented a fluoride release pattern parallel to the control or reference (FLC). The amount of Sr released from the RMGIC decreased with the addition of BAG. Different from the amounts of released F and Sr, the amount of released Al increased with the addition of BAG. Among the 4 types of BAGs, CSP10 provided the most stable F and Sr releases concentrations.

3.4. Attachment, proliferation, and differentiation of cells on the cement

After 5 h of initial incubation, significantly more cells attached on the surface of RMGIC containing BAG (p < 0.05) than on the surface of FLC (Figure 11). Meanwhile, significant differences were found between the surface of RMGIC containing AWG glass and the surfaces of other types of RMGIC containing BAGs. As shown in Figure 12, the proliferation of MC3T3E1 cells on each sample increased with incubation time, and no significant differences were found among the four types of RMGIC containing BAGs and FLC.

Figure 13 summarizes the course of type I collagen, ALP, and osteocalcine mRNA of osteoblasts on each specimen. The expression of type I collagen mRNA for all specimens increased with incubation time. The cements containing BAGs showed a higher differentiation profile than
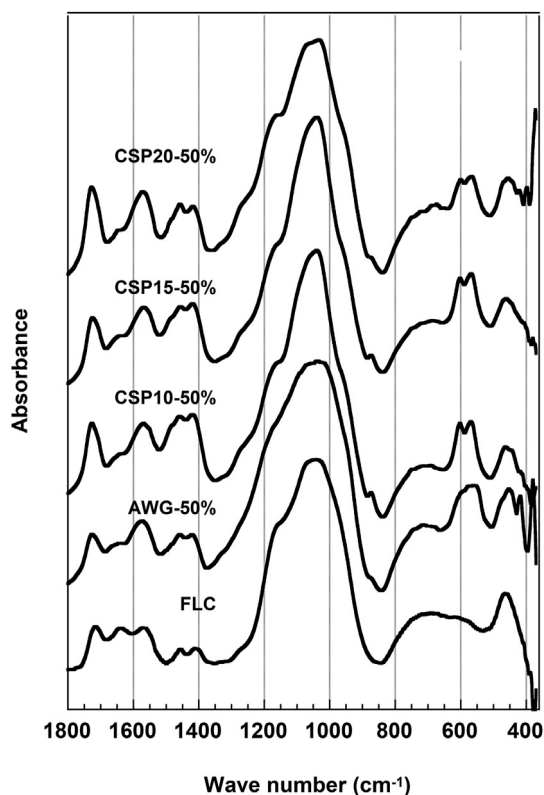
Figure 4. FT-IR spectra of cements containing 50% of bioactive glasses and FLC after 8 weeks of immersion in SBF.
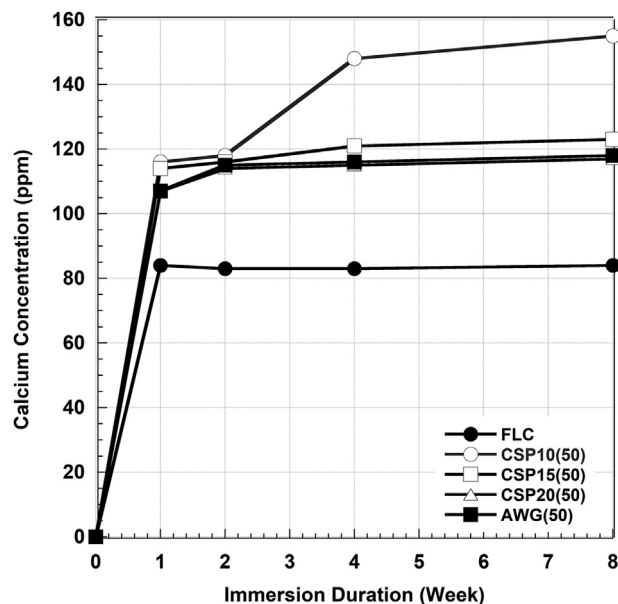

Figure 6. Calcium concentration in the remaining SBF after immersion of the cement without BAG (FLC) and with four types of BAG in 50% for various immersion times.

FLC on the same day. For ALP mRNA, the same phenomena were found with the one of type I collagen mRNA. On day 12, AWG and CSP10 showed the highest ALP mRNA value, CSP15 and CSP20 showed intermediate values, and FLC showed the lowest one.

The gene expression of osteocalcin mRNA in each specimen increased with incubation time. Among all specimens, the increase rate of osteocalcin on AWG was the largest, whereas FLC showed the slowest increase.
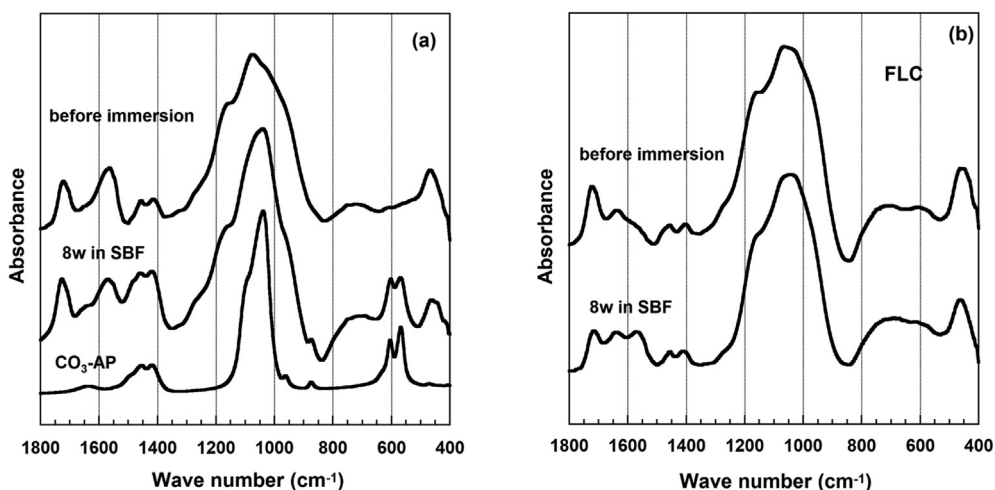

Figure 5. FT-IR spectra for (a) resin-modified glass ionomer cement containing bioactive glass CSP10(50) and (b) FLC before and after 8 weeks of immersion in SBF. Spectra of carbonated hydroxyapatite (CO$_3$-Ap) are used as a reference.

Table 3. Apatite formation in the cements after immersion in SBF 37 °C.

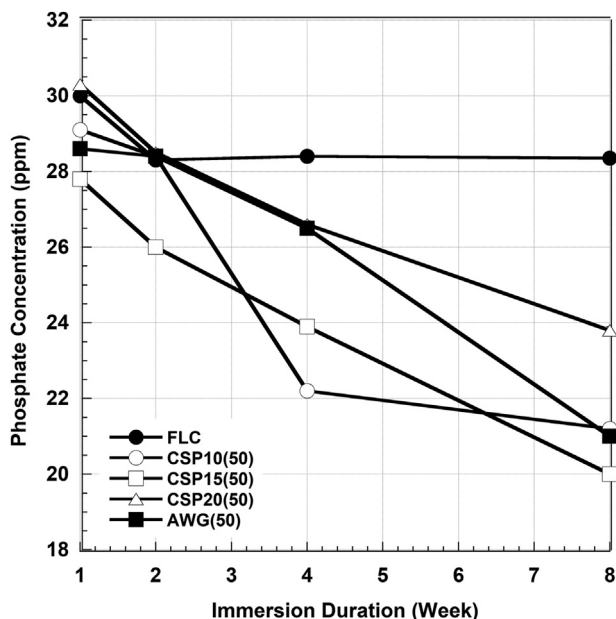| Immersion in SBF (Week)	Apatite Formation by XRD Patterns					Apatite Formation by FT-IR Spectra					Confirmation of Apatite Formation by SEM				
	FLC	CSP10	CSP15	CSP20	AWG	FLC	CSP10	CSP15	CSP20	AWG	FLC	CSP10	CSP15	CSP20	AWG
1	-	-	-	-	-	-	-	-	-	-	-	-	-	-	-
2	-	-	-	-	-	-	-	-	-	-	-	-	-	-	-
4	-	Yes	Yes	Yes	-	-	Yes	Yes	Yes	-	-	Yes	Yes	Yes	-
8	-	Yes	Yes	Yes	Yes	-	Yes	Yes	Yes	Yes	-	Yes	Yes	Yes	Yes

Figure 7. Phosphate concentration in the remaining SBF after immersion of the cement without BAG (FLC) and with four types of BAG in 50% for various immersion times.

As a result, AWG showed significantly ($p < 0.01$) the highest value on days 15 and 21. Other RMGICs containing CSP10, CSP15, and CSP20 showed higher differentiation profiles than FLC, especially on day 21.

4. Discussion

Surface analysis of the specimens of RMGIC containing BAGs revealed that the apatite phase formed after 4 and 8 weeks of immersion in SBF, except for AWG with apatite formation was found only after 8 weeks immersion. The diffraction patterns were typical for all BAG-containing

cements investigated in this study. The peaks were developed around 2θ of $25.5°$ and $32.0°$. The HAP peak around 2θ of $32.0°$ was more prominent, showing higher crystallinity than the cements containing BAGs. This finding suggested that the apatite that formed on the surface of RMGIC containing BAG was poorly crystalline [19, 20]. This fact also allowed RMGIC, which contains less polyacrylic acid than conventional

Figure 9. Log-log plot for strontium (Sr) released in SBF from the reference (FLC without BAG) and cement containing four types of BAG in 50% after various immersion times.

Figure 8. Log-log plot for fluoride (F) released in SBF from the reference (FLC without BAG) and cement containing four types of BAG in 50% after various immersion times.
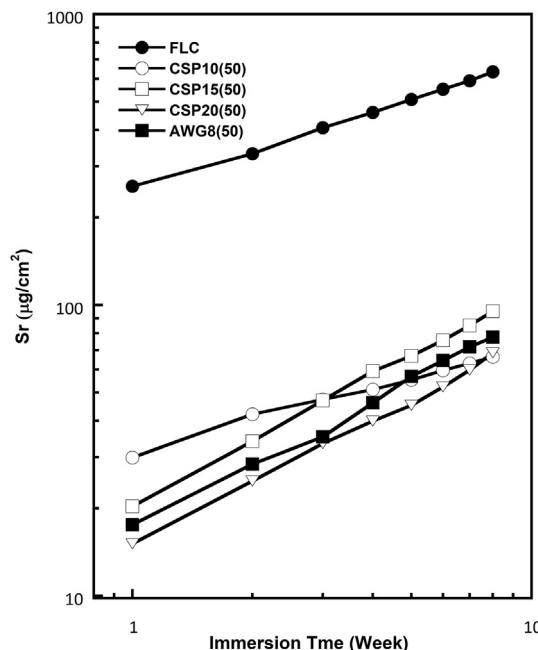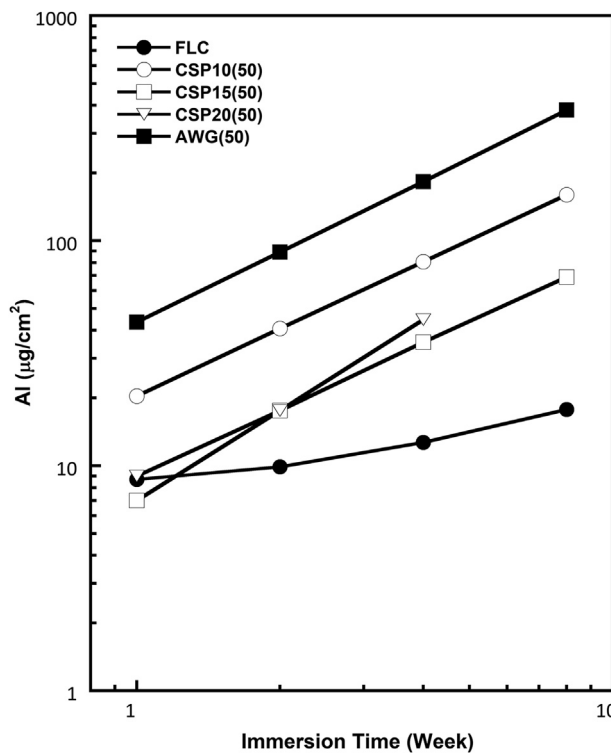

Figure 10. Log-log plot for aluminum (Al) released in SBF from the reference (FLC without BAG) and cement containing four types of BAG in 50% after various immersion times.
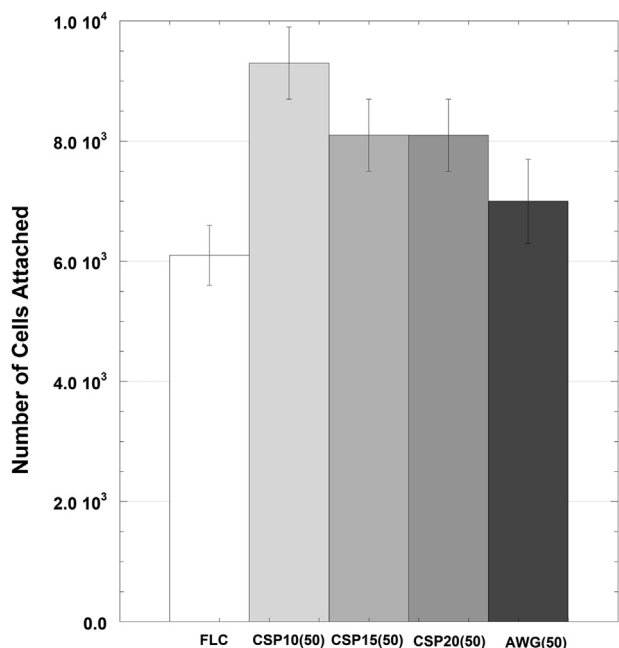
Figure 11. Cell attachment on the surface of FLC and cement containing four types of BAG after 5 h culture (n = 3). Results are shown as the mean $\pm$ standard deviation of the cells attached on the cement disks.
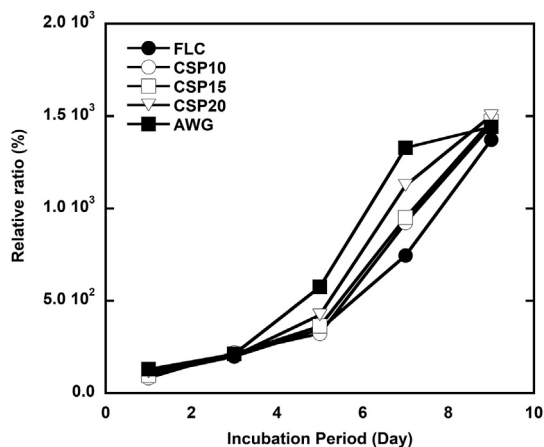

Figure 12. Osteoblast-like cells proliferated on the surface of the FLC and cement containing four types of BAG disks as evaluated by MTT assay. Each value is expressed as a percentage of the amount of absorbance produced by the cells on day 2. The results are shown as the mean $\pm$ standard deviation (n = 9).

GIC, to form an apatite layer on the cement surface after immersion in SBF by incorporation of BAG [20]. In pure $CaO–SiO_2–P_2O_5$ glasses and AW glass ceramics, apatite development occurs after only 7 days of

immersion in SBF [12, 21, 22]. The delayed apatite formation in 4–8 weeks of immersion observed in the present study was probably due to the ratio of BAG compared to the presence of polyacrylic acid inside the cement.

Detection of apatite formation on the bioactive RMGIC was confirmed from the spherical apatite layer found from the micrograph of the samples. Representative bioactive ceramics containing HAP or its components, such as CaO and P_2O_5, can integrate with bone in the body because of apatite-forming ability to act as an interface [23]. However, assessments in SBF implied that CaO and P_2O_5 are not the essential components for the apatite formation [22]. In the $CaO–P_2O_5–SiO_2$ system [24, 25, 26], the $CaO–SiO_2$ system determined the composition of the glass forming an apatite layer in an SBF, and not the $CaO–P_2O_5$ system.

The findings of this study corroborate with previous studies regarding the $CaO–SiO_2$ system. The FT-IR spectra clearly show that the cements containing CSP10(50) and CSP15(50) have a higher ability to form apatite when immersed in SBF, with the development of absorption bands around 873, 602, and 568 cm^{-1} assigned to CO_3 and PO_4 in carbonated apatite aside from the asymmetric stretching vibration of the carboxylates at 1563 cm^{-1}.

The increase in the intensity of a peak at 1563 cm^{-1} assigned to the asymmetric stretching vibration of carboxylate was due to a progress of the acid–base reaction between COOH groups and metal cations, such as Ca^{2+}, Sr^{2+}, and Al^{3+}, by water absorption in the resin matrix [26]. The glass released Ca^{2+} ion from its surfaces via exchange with the H_3O^+ ion in SBF to form Si–OH groups on their surfaces. The functional Si–OH groups were abundant on the surface of cements containing BAG, especially the ones with CSP10(50) and CSP15(50). This fact explains the preferential formation of apatite in those cements. The mechanism of carbonated apatite surface layer formation on the RMGIC containing BAG could be assumed to be the same as that mentioned by Filho *et al.* [27], as described in Table 4.

The concentration of Ca^{2+} ions in SBF increased after certain periods of immersion. The Ca^{2+} ions were released from the cement surface via an exchange with the H_3O^+ ion in the SBF and allowed the formation of Si–OH on their surfaces [23]. Water molecules in the SBF then or simultaneously reacted with the Si–O–Si to form additional Si–OH groups. The Si–OH group induces apatite nucleation, and the released Ca^{2+} ions accelerate apatite nucleation by increasing the ionic activity product of apatite in the fluid [22, 24]. Apatite can grow spontaneously by consuming the calcium and phosphate ions in the surrounding fluid once the apatite nuclei are formed because the SBF is highly supersaturated with respect to apatite [22]. This phenomenon also explains the decrease in phosphate ions with the addition of BAG because the phosphate released was used to form apatite nuclei.

As shown in the results, the fluoride release must have originated entirely from the powder component of the RMGIC. The amount of fluoride releases was also different among the types of BAG, and the order was predicted different depending on the amount of addition. Such a difference cannot be explained at present, and further studies are needed. The slopes of the plots were between 0.35 and 0.51, except for CSP10(50), indicating that the fluoride release was determined by the
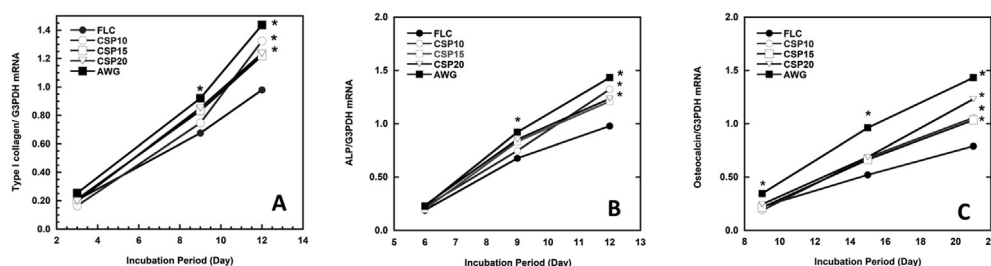

Figure 13. Time course of (A) type I collagen, (B) ALP, and (C) osteocalcin mRNA expressed by MC3T3E1 on each cement specimen. Results are shown as mean $\pm$ standard deviation (n = 9) with p < 0.01. Superscription indicates a significant difference as compared with FLC on the same day.

Table 4. Infrared frequencies for functional groups on a bioactive glass surface before and after SBF reaction [24].

Wave number (cm^{-1})	Vibrational Mode	
1350–1080	P=O	stretch
1250–1100	P=O	associated
940–860	Si–O–Si	stretch
890–800	C–O	stretch
1175–710	Si–O–Si	tetrahedral
610–600	P–O	bend crystal
560–550	P–O	bend amorphous
530–515	P–O	bend crystal
540–4515	Si–O–Si	bend

diffusion process through the cement matrix irrespective of the BAG addition. Fluoride release from restorative materials is clinically important because of its anti-cariogenicity and effect on mineralization [28, 29, 30, 31]. The result found in this study may indicate that that addition of BAG does not interfere fluoride releasing ability of RMGIC.

Meanwhile, Sr release from FLC showed a slope of about 0.44 in the log-log plot, and the release rate was controlled by the diffusion mechanism [32, 33]. However, the addition of BAGs altered the mechanism because the slope increased, except for CSP10. The slope values were about 0.6 and 0.7 in the cements containing 50% BAGs. Sr was possibly involved with the acid–base reaction in the setting process of the cements, and Ca from the BAGs altered the role of Sr by participating in the setting reaction.

The total amount of Al in the cement decreased with the addition of BAG. This fact is closely related to the previous finding that crosslinking of the carboxylates in the polymeric acid by Al proceeds less in the RMGIC containing BAG [15, 33]. The addition of the BAGs caused preferential crosslinking by Ca^{2+} ions in the setting process, and the Al^{3+} ion remained unreacted in the original cement powder or free ion in the cement matrix. This phenomenon may explain the difference in Al release behavior between the cements containing the BAGs and the FLC. The slope in the log-log plot increased to around 1 in the cements containing the BAGs. This fact suggests that the Al release was not diffusion controlled but surface reaction controlled [34]. Due to the content of P_2O_5, it was confirmed that CSP10 with the lowest content of P_2O_5 provided more stable F and Sr ions released.

Cell studies confirmed that BAG addition significantly increased the bioactivity of the RMGIC. The highest attachment was found on the surface of the CSP10(50)-added cement, but no difference in cell proliferation was found among the cements with different types of BAG added. Previous studies demonstrated that surface topology of the substrate is a factor affecting osteoblast attachment. Surface topology represented by surface composition and structure influences the kinetics of protein adsorption and the structure of the adsorbed protein [35, 36, 37, 38, 39, 40], thus influencing the attachment of osteoblasts. In the present study, significant differences between FLC and the other set cements could be explained by the apatite development on the surface of the RMGIC containing BAGs.

Chang et al. [39] reported that the affinity of serum protein components for HAP surfaces is so high so that no apparent differences could be found among the three HAP surfaces. In the present study, we found a significant difference between the cement containing AWG and three other types of RMGIC containing BAG. This result needs further investigation.

Cell differentiation toward bone mineralization was higher on the cement containing BAG, as indicated by type I collagen, ALP, and osteocalcin markers. The results were corroborated with the report from Ozawa and Kasugai [40] that ALP activity and the number of mineralized nodules by rat bone marrow stromal cells are higher on bioactive surface. Hott et al. [36] demonstrated that collagen synthesis and calcium uptake by osteoblastic cells are higher on HAP and they speculated that the differentiation of osteoblastic cells can be enhanced slightly on HAP. The results of this study with respect to the RMGICs containing BAGs in comparison with FLC were consistent with their results. In other words, differentiation of osteoblasts was enhanced on the surface of the RMGICs containing BAGs. The gene expression of type I collagen, ALP, and osteocalcin mRNA in the four types of RMGIC containing BAGs were greater than those on FLC.

5. Conclusion

RMGIC containing BAG shows adequate bioactivity through carbonate apatite formation on its surface when immersed in SBF. The apatite formed was poorly crystalline, which has better bone bonding ability. The addition of BAG to RMGIC did not affect fluoride release, which is responsible for the inhibition of demineralization. Results of Sr and Al analyses revealed that BAG addition may not influence the matrix stability of RMGIC. The increase in Ca release with the addition of BAG is a positive factor indicating excellent ion exchange with the SBF. Furthermore, the decrease in P concentration may indicate that apatite formation might grow spontaneously by consuming the Ca and P ions in the surrounding fluid. The osteoblast differentiation on the four types of RMGIC containing BAGs was higher than that on FLC but was the same in all types of RMGIC containing BAG. This result may indicate that all types of cement containing BAG are osteoconductive. The newly developed RMGIC containing BAG provides new insights into the development of new generation of cement for biomedical purposes.

References

[1] A.D. Wilson, B.E. Kent, The glass ionomer cement: a new translucent dental filling material, J Appl Chem Biotechnol 21 (1971) 313–320.

[2] E.M. Benelli, M.C. Serra, A.L. Rodriguez, J.A. Curry, In situ anticariogenic potential of glass-ionomer cement, Caries Res. 27 (1993) 280–284.

[3] H. Forss, L. Seppa, Prevention of enamel demineralization adjacent to glass-ionomer filling materials, Scand. J. Dent. Res. 98 (1990) 173–178.

[4] J.W. McLean, J.W. Nicholson, A.D. Wilson, Guest Editorial: proposed nomenclature for glass-ionomer dental cements and related materials, Quintessence Int. 25 (1994) 587–589.

[5] E. Cho, H. Kopel, S.N. White, Moisture susceptibility of resin-modified glass ionomer materials, Quintessence Int. 26 (1995) 351–358.

[6] A.D. Wilson, Resin-modified glass ionomer cements, Int. J. Prosthodont. (IJP) 3 (1990) 425–429.

[7] I.M. Brook, P.V. Hatton, Glass- ionomers: bioactive implant materials, Biomaterials 19 (1998) 565–571.

[8] A.U.J. Yap, Y.S. Pek, R.A. Kumar, P. Cheang, K.A. Khor, Experimental studies on a new bioactive material: HA Ionomer cements, Biomaterials 23 (2002) 955–962.

[9] H. Yli-Urpo, L.V.J. Lassila, T. Narhi, P.K. Vallitu, Compressive strength and surface characterization of glass ionomer cements modified by particles of bioactive glass, Dent. Mater. 21 (2005) 201–209.

[10] S. Matsuya, Y. Matsuya, M. Ohta, Structure of bioactive glass and its application to glass- ionomer cement, Dent. Mater. J. 18 (2) (1999) 155–166.

[11] A. Valanezhad, T. Odatsu, K. Udoh, T. Shiraishi, T. Sawase, I. Watanabe, Modification of resin modified glass ionomer cement by addition of bioactive glass nanoparticles, J. Mater. Sci. Mater. Med. 27 (1) (2016) 1–9.

[12] T. Kokubo, Bioactive glass ceramics: properties and applications, Biomaterials 12 (1991) 155–163.

[13] P.K. Vallittu, A.R. Boccaccini, L. Hupa, D.C. Watts, Bioactive dental materials - do they exist and what does bioactivity mean? Dent. Mater. 34 (5) (2018) 693–694.

[14] M. Kamitakahara, M. Kawashita, T. Kokubo, T. Nakamura, Effect of polyacrylic acid on the apatite formation of bioactive ceramic in a simulated body fluid: fundamental examination of the possibility of obtaining bioactive glass-ionomer cements for orthopedic use, Biomaterials 22 (2001) 3191–3196.

[15] I.D. Ana, S. Matsuya, M. Ohta, K. Ishikawa, Effects of added bioactive glass on the setting and mechanical properties of resin- modified glass ionomer cement, Biomaterials 24 (2003) 3061–3067.

[16] T. Kokubo, H. Takadama, How useful is SBF in predicting in vivo bone bioactivity? Biomaterials 27 (2006) 2907–2915.

[17] T. Yuasa, Y. Miyamoto, K. Ishikawa, M. Takechi, Y. Momota, S. Tatehara, M. Nagayama, Effects of apatite cements on proliferation and differentiation of human osteoblasts in vitro, Biomaterials 25 (7-8) (2004) 1159–1166.

[18] M.M. Bradford, A rapid and sensitive method for the quantitation of microgram quantities of protein utilizing the principle of protein-dye binding, Anal. Biochem. 7 (72) (1976) 248–254.

[19] R.Z. Le Geros, Calcium Phosphates in Oral Biology and Medicine, Karger, Basel, 1991, pp. 5–6.

[20] J.C. Elliot, Structure and Chemistry of the Apatites and Other Calcium Orthophosphates, Elsevier Science BV, Amsterdam, 1994, p. 310.

[21] S. Matsuya, T. Maeda, M. Ohta, ^{23}Na, ^{27}Al, ^{29}Si and ^{31}P MAS NMR spectroscopy of setting reaction of the glass ionomer cement, Bioceramics 9 (1996) 461–464.

[22] C. Ohtsuki, T. Kokubo, T. Yamamuro, Mechanism of HA formation of CaO-SiO$_2$-P$_2$O$_5$ glasses in simulated body fluid, J Non Crys Solid 143 (1992) 84–92.

[23] T. Kokubo, H. Kushitani, S. Sakka, T. Kitsugi, T. Yamamuro, Solutions able to reproduce in vivo surface structure changes in bioactive glass ceramic A-W, J. Biomed. Mater. Res. B Appl. Biomater. 53 (2000) 28–35.

[24] K. Ohura, T. Yamamuro, T. Nakamura, T. Kokubo, Y. Ebisawa, Y. Kotoura, M. Oka, Bone- bonding ability of P$_2$O$_5$- free CaO.SiO$_2$ glasses, J. Biomed. Mater. Res. 25 (1991) 357–365.

[25] H.M. Kim, F. Miyaji, T. Kokubo, M. Kobayashi, T. Nakamura, Bioactivity of M$_2$O-TiO$_2$-SiO$_2$ (M=Na, K) glasses, an in vitro evaluation, Bull. Chem. Soc. Jpn. 69 (1996) 2387–2394.

[26] A.M. Young, FTIR investigation of polymerization and polyacid neutralization kinetics in resin-modified glass-ionomer dental cements, Biomaterials 23 (2002) 3289–3295.

[27] O.P. Filho, G.P. La Torre, L.L. Hench, Effect of crystallization on apatite layer formation of bioactive glass 45S5, J. Biomed. Mater. Res. 30 (1996) 504–514.

[28] L. Forsten, Fluoride release and uptake by glass- ionomers and related materials in its clinical effect, Biomaterials 19 (1998) 503–508.

[29] C. Francci, T.G. Deaton, R.R. Arold, E.J. Swift Jr., J. Perdigao, J.W. Bawden, Fluoride release from restorative materials and its effects on dentin demineralization, J. Dent. Res. 78 (10) (1999) 147–154.

[30] Y. Momoi, J.F. Mc Cabe, Fluoride release from light activated glass ionomer restorative cements, Dent. Mater. 9 (1993) 151–154.

[31] R.M.H. Verbeeck, E.A.P. De Maeyer, L.A.M. Marks, R.J.G. De Moor, A.M.J.C. De Witte, L.M. Trimpeneer, Fluoride release process of (resin-modified) glass- ionomer cements versus (polyacid-modified) composite resin, Biomaterials 19 (1998) 509–519.

[32] P.Z. Gao, S. Matsuya, M. Ohta, J.Z. Zhang, Erosion process of conventional and light- cured glass ionomer cements in citrate buffer solution, Dent. Mater. J. 16 (1) (1997) 170–179.

[33] D. Sales, D. Sae-Lee, S. Matsuya, I.D. Ana, Short term fluoride and cations release from polyacid-modified composites in a distilled water and an acidic lactate buffer, Biomaterials 24 (2003) 1687–1696.

[34] M. Fukazawa, S. Matsuya, M. Yamane, The mechanism of erosion of glass ionomer cements in organic acid buffer solutions, J. Dent. Res. 69 (1990) 1175–1179.

[35] D.A. Puleo, L.A. Holleran, R.H. Doremus, R. Bizios, Osteoblast responses to orthopedic implant materials in vitro, J. Biomed. Mater. Res. 25 (1991) 711–723.

[36] M. Hott, B. Noel, D. Bernache-Assolant, C. Rey, P.J. Mary, Proliferation and differentiation of human trabecular osteoblastic cells on hydroxyapatite, J. Biomed. Mater. Res. 72 (1997) 248–254.

[37] H. Zreiqat, P. Evans, C.R. Howlett, Effect of surface chemical modification of bioceramic on phenotype of human bone- derived cells, J. Biomed. Mater. Res. 44 (1999) 389–396.

[38] D.D. Deligianni, N.D. Katsala, P.G. Koutsoukos, Y.F. Missirlis, Effect of surface roughness of hydroxyapatite on human bone marrow cell adhesion, proliferation, differentiation, and detachment strength, Biomaterials 22 (2001) 87–96.

[39] Y.L. Chang, C.M. Stanford, J.S. Wefel, J.C. Keller, Osteoblastic cell attachment to hydroxyapatite coating implant surface in vitro, Int. J. Oral Maxillofac. Implants 14 (1999) 239–247.

[40] S. Ozawa, S. Kasugai, Evaluation of implant materials (hydroxyapatite- glass ceramics, titanium) in rat bone marrow stromal cell culture, Biomaterials 17 (1996) 23–29.